Full-Scale Pseudodynamic Testing of Self-Centering Steel Plate Shear Walls

Daniel M. Dowden, P.E., S.E.[1]; Patricia M. Clayton, M.ASCE[2]; Chao-Hsien Li[3]; Jeffrey W. Berman, A.M.ASCE[4]; Michel Bruneau, F.ASCE[5]; Laura N. Lowes, M.ASCE[6]; and Keh-Chyuan Tsai[7]

Abstract: This paper presents the first full-scale experimental investigation of the self-centering steel plate shear wall (SC-SPSW) system. The SC-SPSW system is a lateral force-resisting system developed to provide system recentering and limit structural damage to easily replaceable energy dissipating fuses (i.e., thin steel web plates). Recentering is provided by posttensioned (PT) beam-to-column connections. This test program is composed of two two-story SC-SPSW specimens, each with a different PT beam-to-column connection. For one specimen, connections rock about both beam flanges; for the other, connections rock about the top beam flange only. Both specimens incorporated a posttensioned column base detail to further promote recentering and damage mitigation. The specimens were tested pseudodynamically using excitations representing three different seismic hazard levels. Results show that the SC-SPSW system is capable of meeting and exceeding the specified performance objectives. **DOI: 10.1061/(ASCE)ST.1943-541X.0001367.**

Author keywords: Self-centering; Steel plate shear wall; Large-scale testing; Pseudodynamic testing; Seismic effects.

Introduction

The self-centering steel plate shear wall (SC-SPSW) concept has been proposed as a lateral force-resisting system capable of reducing the economic impact of earthquakes by providing system recentering and by limiting ductile yielding to easily replaceable energy dissipating steel infill plates (Dowden et al. 2012; Clayton et al. 2012a, b). In the SC-SPSW, the infill plates, referred to as web plates, resist lateral load through the development of tension field action and provide energy dissipation through ductile web plate yielding. Posttensioned (PT) beam-to-column and column base connections provide system recentering capabilities while still retaining the high strength and initial stiffness characteristics of SPSWs.

Clayton et al. (2012a) proposed a performance-based seismic design (PBSD) procedure for SC-SPSWs with the following performance objectives:

1. *No repair* required after an earthquake with 50% probability of exceedence in 50 years (50/50);
2. *Repair of web plates only* and recentering after a 10% in 50 year earthquake (10/50); a target drift ratio limit was established at 2% based on code-based drift limits (ASCE 2010); and
3. *Collapse prevention* after a 2% in 50 year earthquake (2/50); a target drift limit was established at 4%, based on engineering judgment and the drift at which test data show significant strength loss for conventional SPSWs (Baldvins et al. 2012).

To meet these target performance objectives, a step-by-step design procedure was developed by Clayton et al. (2012a) based on capacity design principles. Using this procedure, the web plates are proportioned for design-level earthquake forces from the 10/50 base shear demands, reduced by the response modification factor, R, which is taken equal to that of a conventional steel plate shear wall. Then, the boundary frame members are capacity designed for the strength demands of the yielded web plates and elastic PT force demands at a target drift associated with the 2/50 event (Dowden et al. 2012). This design procedure was verified through nonlinear response history analyses of three-story and nine-story prototype buildings having SC-SPSW designs with different numbers of beam PT strands, values of the initial PT force, infill web plate thicknesses, and sizes of the beam and column boundary frame members. The results confirmed that the SC-SPSW so designed were able to meet the target performance objectives at the 10/50 and 2/50 seismic hazard levels. Furthermore, quasi-static cyclic testing of SC-SPSW subassemblies (Clayton et al. 2012b) and third-scale three-story specimens (Dowden and Bruneau 2014) have shown good agreement with simple numerical models.

This paper presents test results from an experimental program conducted to validate the SC-SPSW seismic performance at full scale; the corresponding analytical investigation and numerical results can be found in Clayton et al. (2015) and Dowden and Bruneau (2014). Two full-scale two-story SC-SPSW specimens were tested pseudodynamically with earthquake excitations representing the aforementioned seismic hazard levels; testing was conducted at the National Center for Research on Earthquake Engineering (NCREE) in Taiwan. The specimens, designated as

[1]Research Engineer, Structural Engineering and Earthquake Simulation Laboratory, Dept. of CSEE, Univ. at Buffalo, Buffalo, NY 14260 (corresponding author). E-mail: dmdowden@buffalo.edu

[2]Assistant Professor, Dept. of Civil, Architectural, and Environmental Engineering, Univ. of Texas at Austin, Austin, TX 78712. E-mail: clayton@utexas.edu

[3]Assistant Research Fellow, National Center for Research on Earthquake Engineering, No. 200, Sec. 3, Xinhai Rd., Taipei 10617, Taiwan. E-mail: chli@ncree.narl.org.tw

[4]Associate Professor, Dept. of CEE, Univ. of Washington, Seattle, WA 98145. E-mail: jwberman@uw.edu

[5]Professor, Dept. of CSEE, Univ. at Buffalo, Buffalo, NY 14260. E-mail: bruneau@buffalo.edu

[6]Associate Professor, Dept. of CEE, Univ. of Washington, Seattle, WA 98145. E-mail: lowes@uw.edu

[7]Professor, Dept. of Civil Engineering, National Taiwan Univ., Taipei 10617, Taiwan. E-mail: kctsai@ntu.edu.tw

Note. This manuscript was submitted on November 2, 2014; approved on June 9, 2015; published online on July 8, 2015. Discussion period open until December 8, 2015; separate discussions must be submitted for individual papers. This paper is part of the ***Journal of Structural Engineering***, © ASCE, ISSN 0733-9445/04015100(10)/$25.00.

FR and NZ, incorporated two different PT beam-to-column connection details. The flange-rocking (FR) connection (Clayton et al. 2012a, b; Dowden et al. 2012), which results in rocking about the top or bottom beam flange depending on the loading direction, has been employed in previous self-centering moment-resisting frame studies (e.g., Christopoulos et al. 2002; Garlock et al. 2005). The NewZ-BREAKSS (NZ) connection, which results in rocking about the top beam flange only, was proposed by Dowden and Bruneau (2011), who were inspired by connections proposed previously by others (e.g., Clifton et al. 2007; MacRae et al. 2009; Mander et al. 2009; Khoo et al. 2011), to eliminate the PT boundary frame expansion (i.e., increase in distance between frame column centerlines) that occurs with flange-rocking connections; this results in reduced frame stiffness and reduced recentering capacity compared to the FR connection. Both specimens incorporated a PT column base detail to provide additional recentering capabilities and prevent plastic hinging at the column base.

Prototype Building and Design

The SC-SPSW specimens were designed following the performance-based design procedure proposed in Clayton et al. (2012a), with slight modifications noted in the following. The specimens were designed to be the lateral force-resisting system for a regular two-story building located in a region of high seismicity. This prototype building had the same plan dimensions, story heights, story masses, and loading as the bottom two stories of the three story building used in the SAC Steel Project (FEMA 2000). The building was located in Los Angeles, with target spectral response values at various periods as presented in FEMA (2000) and in Clayton et al. (2012a). The 10% in 50-year hazard level was assumed to approximate a design-basis earthquake (DBE) (Somerville et al. 1997), resulting in short-period and 1-s-period spectral response acceleration parameters, S_{DS} and S_{D1}, of 1.07 and 0.68, respectively.

The seismic mass attributed to each specimen was based on a preliminary design of the prototype building. As an initial design step, the target strength of Specimen FR at design-level drift demands was assumed equal to that of a conventional SPSW with similar frame dimensions that was tested previously at NCREE [approximately 1,400 kN at 2% roof drift (Li et al. 2014)]. This was done to enable reuse of existing NCREE testing equipment. The design strength of the specimen was then estimated to be 700 kN assuming an overstrength factor, Ω_o, of 2 for conventional SPSWs. From this, it was determined that four SC-SPSW specimens would be required in each principle direction of the building to resist design-level seismic loads. Finally, specimen strength was determined considering actual web plate material properties (described in the following section) and the contribution of both the infill web plate and the PT boundary frame using the principle of virtual work, assuming yielded web plates and PT connection flexural strengths equal to the moment at decompression, along with appropriate strength reduction factors (Clayton 2013). Accordingly, the preliminary number of lateral frames was found to be appropriate, leading to a total tributary frame seismic mass of 473,000 kg or approximately one-fourth of the total building mass.

To simplify test frame fabrication as well as to facilitate comparison of experimental results for the two specimens, it was desired that Specimens FR and NZ be nominally identical, with the exception of the beam-to-column connections. Differences in the PT beam-to-column connections were estimated (by nonlinear cyclic pushover analysis) to reduce the Specimen NZ strength by approximately 25% in comparison with Specimen FR. The difference in strengths arises mainly due to the presence of the initial PT beam-to-column decompression moment effects inherent with Specimen FR, which is not present with Specimen NZ. That is, for Specimen FR, the frame joints behave as rigid connections prior to the formation of a gap between the beam and column flanges, since both the top and bottom beam flanges are in contact with the columns. For Specimen NZ, this does not occur because the NewZ-BREAKSS connection is detailed with an initial gap between the beam bottom flanges and the columns. Accordingly, the seismic mass of Specimen NZ, for numerical simulation of the pseudodynamic tests, was reduced by 25% from that of Specimen FR.

It should be noted that the performance-based seismic design (PBSD) procedure presented in Clayton et al. (2012a) recommends designing the web plate to resist the entire seismic story shear. Here, however, a less conservative, balanced design approach was employed in which seismic story shear was assumed to be resisted by both the web plate and the boundary frame. Thus, the specimens are *underdesigned* with respect to the PBSD procedure by Clayton et al. (2012a) that considers only web plate strength. While this balanced design approach is not being proposed for future SC-SPSW design, the test results presented herein should be interpreted in the context that the specimens represent the results of a feasible but less conservative design methodology.

Test Specimens and Setup

The final design for Specimens FR and NZ is shown in Fig. 1. As discussed earlier, only the beam-to-column joint detail is different between the two specimens. Special detailing of PT beam-column and column-base connections (as shown in Fig. 1) was required to accommodate rocking. For the PT beam-column connections at the middle and top beam locations, a shear plate with horizontally slotted bolt holes was used to accommodate relative joint rotations and to resist beam shear forces; a bolted double-angle connection at the bottom beam was used to achieve a similar behavior. Furthermore, the PT column-base connection is similar to that used in previously tested self-centering moment-resisting frames (Chi and Liu 2012), follows the same kinematics as the Specimen FR beam-to-column rocking joint connections, and provides additional restoring forces for postevent system recentering. In the PT column-base detail, the column uplift force is resisted by vertical PT rods and the horizontal shear forces are resisted by the bolted shear brackets. The vertical PT rods are anchored in the columns, just above the middle beam connection (as shown Fig. 1). The placement of the PT anchorage was governed by available load cell capacities for testing, but PT anchorage could be placed elsewhere within the first story height to meet SC-SPSW design objectives. Alternatively, a clevis column-base detail could also be used (Dowden and Bruneau 2014) to allow free rotation of the column base (but without additional restoring forces for recentering).

Material properties specified for the SC-SPSW frames consisted of A992 steel ($F_y = 345$ MPa) for the boundary frame members, low yield strength 225 ($F_y = 225$ MPa) steel panels for the web plates, A416 Grade 270 seven-wire strands ($F_u = 1{,}860$ MPa) for the beam PT strands, and high-strength threaded rod ($F_u = 1{,}030$ MPa) for the column PT bars. Coupons of the infill web plate material were extracted in the longitudinal, transverse, and 45° directions with respect to the plate roll direction. The mechanical properties of the coupon in the longitudinal direction provided an upper-bound representation of the expected strength of the infill web plate, results of which are shown in Fig. 2. Material coupon tests for the boundary frame and PT elements were not

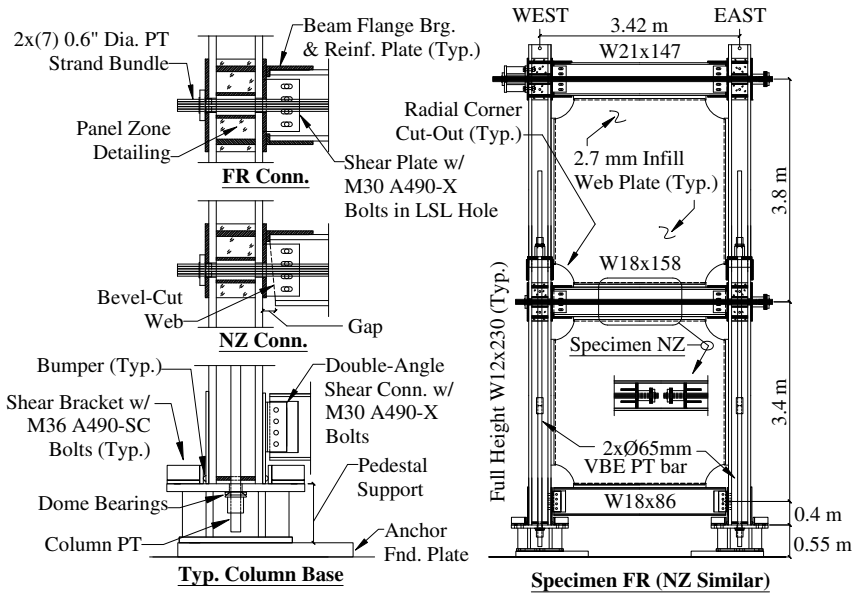

Fig. 1. Schematic of test specimens

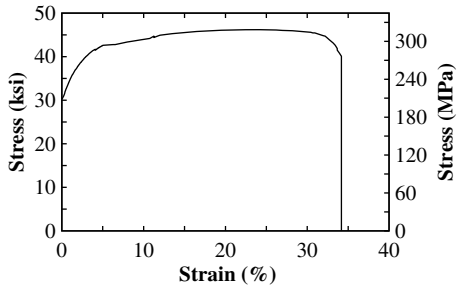

Fig. 2. Web plate coupon

performed as it was expected that these members would remain essentially elastic.

For the beam PT, an initial PT force of approximately 30% of the yield strength (with yield taken as $0.9 \times F_u$) of the PT strands was targeted for both test specimens. For the column PT, approximately 25% and 15% of yield were targeted for Specimen FR and NZ, respectively. The difference in levels of initial PT column force provided between the two frames was a coordination oversight during the testing program (as ideally the initial PT force would have been identical). The only significance of this difference is that Specimen NZ will have a lesser overall recentering response than Specimen FR. The PT strands were tensioned using a hydraulic jack system and some PT force losses due to anchor wedge seating and elastic beam shortening were expected. Therefore, the strands were overstressed slightly prior to releasing the hydraulic jack system, meaning the target PT forces were only approximately achieved.

Figs. 3 and 4 show a schematic of the test setup and a typical test specimen during testing (shown for a positive drift demand), respectively. As indicated in the figures, lateral loading for the specimens was provided by direct attachment of two actuators (1,000-kN capacity each) to the top of the west column using a transfer beam to accommodate the beam PT anchorage on the outside of the column flange. The SC-SPSW test specimens were laterally braced by a steel modular frame and anchorage system. The modular steel frame provided out-of-plane restraint but allowed the frame to move freely in-plane by allowing the test specimen to slide on a lubricated interface between the lateral bracing frame columns and contact points along the beam flanges. Contact points of the SC-SPSW test frame were provided by T-brace

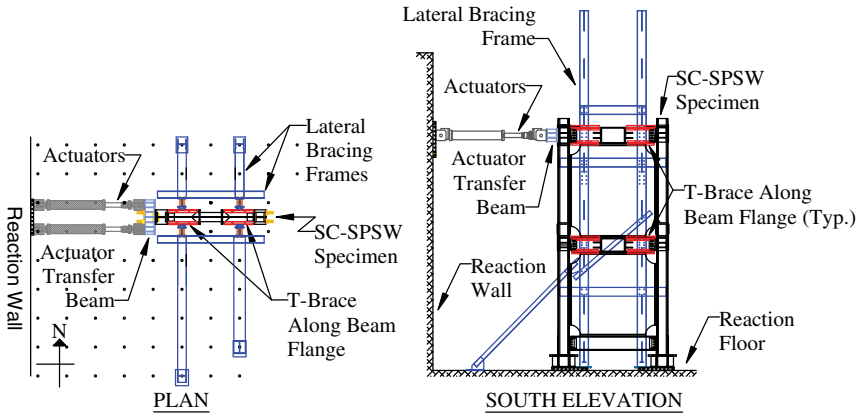

Fig. 3. Experimental test setup

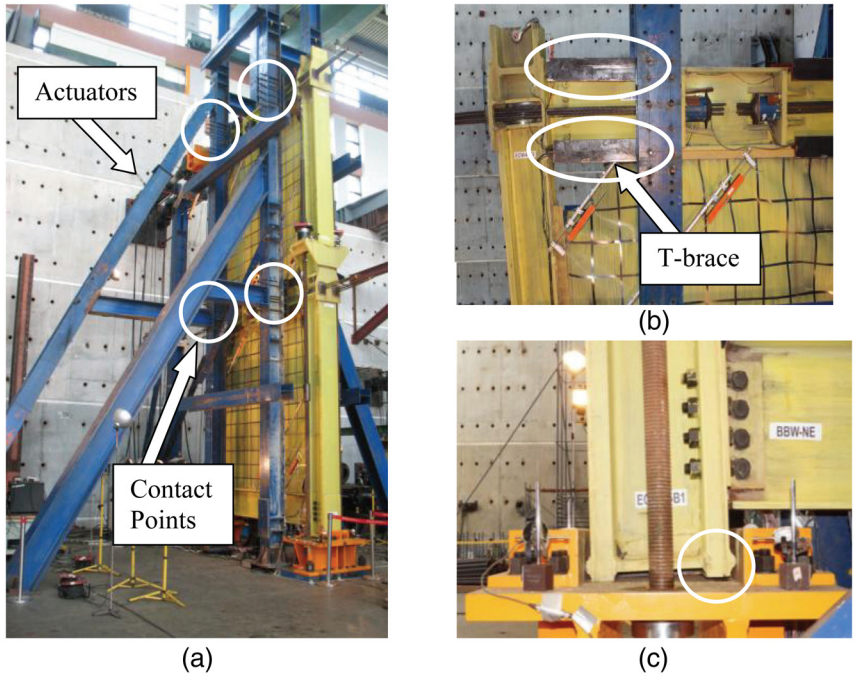

Fig. 4. (a) Specimen NZ; east column positive drift; (b) joint; (c) column base rocking

sections (1,000 mm in length each) at each ends of the middle and top beams at both top and bottom flanges. Instrumentation was provided to record local and global responses and included displacement transducers, load cells, and strain gauges. Additional information on the test setup and instrumentation is provided in Clayton (2013) and Dowden and Bruneau (2014).

Pseudodynamic Loading

For both specimens, the loading protocol consisted of pseudodynamic (PSD) and quasi-static cyclic tests. The test sequence was as follows: an elastic PSD free vibration test starting at a roof displacement of 10 mm (approximately 0.13% drift); an elastic cyclic test of two cycles at 0.15% roof drift; PSD tests representing seismic hazard levels of 50, 10, and 2% probability of exceedence in 50 years (50/50, 10/50, 2/50, respectively); and inelastic cyclic tests. The inelastic cyclic test for Specimen FR consisted of two cycles of loading at 4.5% drift; the inelastic cyclic tests for Specimen NZ consisted of two cycles of loading at increasing drift values starting at 2.5% and increasing up to 4.5% drift in increments of 0.5% drift, and the 4.5% drift cycle was repeated an additional three cycles. For both specimens, no repairs were made between tests. This is significant for interpreting the results of the 2/50 tests, as the web plates yielded and developed minor tears during the 10/50 tests.

Ground acceleration records for the PSD tests were selected from the SAC ground motion (GM) suite for Los Angeles (Somerville et al. 1997) to represent the three seismic hazard levels. For each hazard level, nonlinear analyses of the prototype building were conducted using the appropriate set of SAC GMs and the modeling procedures in Clayton et al. (2012a). Using these results, an individual record was identified that resulted in a maximum roof drift near the median maximum roof drift for each hazard-specific set of GMs. This motion was used for the PSD experimental tests. For the 2/50 hazard level, a *near median* maximum roof drift was achieved by amplitude scaling the LA23 motion by a factor of 1.3. Table 1 provides information for the GMs used in the laboratory tests. Only the portion of the GM representing strong shaking was used for the tests to reduce test duration without significantly affecting peak drift demands. To investigate postevent response including recentering, each excitation was followed by a period of free vibration, the duration of which is provided in Table 1.

Fig. 5 shows the elastic response spectra for the excitations used in the PSD experimental tests as well as the MCE and design spectra. The MCE spectrum is defined by the FEMA (2000) 2/50 spectral values; the design spectrum is defined as 2/3 of the MCE spectrum per ASCE 7 (ASCE 2010). Also shown in Fig. 5 by a vertical dotted line is the approximate initial fundamental period, T_i, for the test specimens (discussed in the following section). It should be noted that the 10/50 and 2/50 PSD spectra are larger than the design and MCE target spectra, respectively.

Table 1. Summary of Ground Motions in Pseudodynamic Tests

		Time window (s)				Free vibration (s)	
Test	SAC motion	Begin	End	Scale	PGA[a] (g)	Specimen FR	Specimen NZ
50/50	LA42	2.59	4.85	1	0.33	3.00	5.41
10/50	LA01	0	15.18	1	0.46	2.73	4.82
2/50	LA23	4.01	14.14	1.3	0.54	7.02	7.06

[a]PGA is for excitation after scale factor is applied.

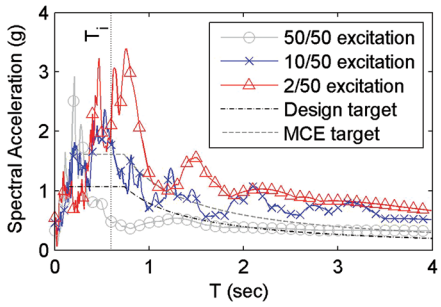

Fig. 5. Excitation and target response spectra for PSD tests

The PSD tests assumed the specimen to be a single-degree-of-freedom system with a lumped mass equal to the seismic mass of both stories of the structure located at the height of the actuators and an instantaneous stiffness determined from the measured specimen response. The Newmark (1959) explicit integration method was used in the PSD loading protocol with an analytical time step of 0.01 s. Ground acceleration records were linearly interpolated to match the PSD time step. Initial free vibration tests (presented later) of both specimens indicated approximately 1 and 4% inherent damping in the FR and NZ test specimens, respectively. This was judged to be already a significant level of equivalent damping, particularly for steel buildings (Villaverde 2009), so no additional numerical damping was included in the PSD tests to ensure conservative results for the displacement response.

Experimental Results

Free Vibration Response

Elastic PSD-free vibration tests were performed before conducting the earthquake simulation tests to determine the approximate initial period and equivalent viscous damping for the two specimens. The results are provided in Table 2, where the viscous damping ratios were obtained using the logarithmic decrement procedure (Chopra 2007). As indicated, Specimen NZ exhibited significantly more damping than Specimen FR. While the reason for this disparity in initial damping ratio could not be explained, one possible source could be due to friction in the NZ connections that rock under initial loading (i.e., for Specimen FR, the beam-to-column joints remained closed during the elastic PSD free vibration tests).

Note that the purpose of the free vibration tests was to obtain an approximate value of equivalent viscous damping to use in the PSD algorithm for testing purposes. As indicated earlier, it was determined that no additional numerical damping was necessary for use in the integrator for solving the incremental equations of motion, so no additional numerical damping was included in the PSD tests to ensure conservative results for the displacement response. Accordingly, the values of viscous damping reported are not necessarily representative of the SC-SPSWs in an actual building, but a consequence of the test setup.

Global Response

The global response, in terms of base shear force versus roof drift, of the test specimens during the dynamic loading are shown in Fig. 6. The peak roof drifts and residual drifts for each specimen and each GM are given in Table 2. For both specimens, story drifts were approximately equal to roof drift throughout the test. Periodic pauses in testing were made to provide visual assessment of the specimens. Global response data and documented visual assessment support the following observations:

1. For the 50/50 GM, the test specimens remained essentially elastic with indications of minor web plate yielding. Peak roof drifts were less than 0.5% drift for both specimens. As anticipated, Specimen FR had a larger stiffness than Specimen NZ. This is due to the decompression moment effects of the closed beam-to-column PT connection at small drift demands, which is not present for Specimen NZ (for reasons noted earlier).
2. For the 10/50 GM, some web plate tearing was observed in both specimens. Onset of infill web plate tearing is attributed to the development of large tensile strains at the corners of the infill web plate due to localized stress concentrations and out-of-plane buckling along the plastically elongated free-edge of the infill plate corner cut-outs, which is further exacerbated by the formation of a gap at the beam-to-column joints. A proposed analytical equation to facilitate joint detailing to delay such tearing effects can be found in Dowden and Bruneau (2014). Tearing initiated at the corners of the web plates near the boundary frame; Fig. 7(a) shows an example tear at the upper east corner of the first-story web plate along the middle beam following a peak roof drift demand of approximately 2% for Specimen NZ. Web plate tearing did not have a significant effect on specimen strength [Fig. 6(b)]. This is because tearing was minimal and the increase in PT frame strength with increasing drift demands was greater than the losses due to web plate tearing. Minor localized yielding on the boundary frame was also observed in both specimens during the 10/50 GM. Fig. 7(b) shows minor yielding at the location of the PT anchorage in the top beam of Specimen NZ. The peak roof drifts reached approximately 2%. Residual drifts, determined from the decayed GM free vibration response, were less than 0.2%, which is the threshold for recentering considered and corresponds to the out-of-plumb tolerances for new construction.
3. For the 2/50 GM, additional web plate tearing was observed. Fig. 7(c) shows an example of tearing at the upper east corner of the first-story web plate following a peak roof drift of approximately 4.6% for Specimen FR. Despite this tearing, the majority of the web plate remained attached to the boundary frame. Cumulative localized yielding in the boundary frame was insignificant, and the boundary frames remained essentially elastic for the 2/50 GM. Fig. 7(d) shows typical limited yielding on the east column just below the web doubler plates at the connection with the middle beam after completion of all PSD and inelastic cyclic tests (of which the base shear versus roof drift results are presented in Fig. 8). The data in Table 2

Table 2. Summary of Pseudodynamic Test Results

Specimen	Seismic mass (kg)	Initial period (s)	Initial damping ratio (%)	Absolute maximum roof drift (%)			Absolute maximun residual roof drift (%)	
				50/50	10/50	2/50	10/50	2/50
FR	473,000	0.58	0.91	0.25	1.97	4.56	0.05	0.10
NZ	354,750	0.60	4.10	0.30	2.00	4.70	0.10	0.41

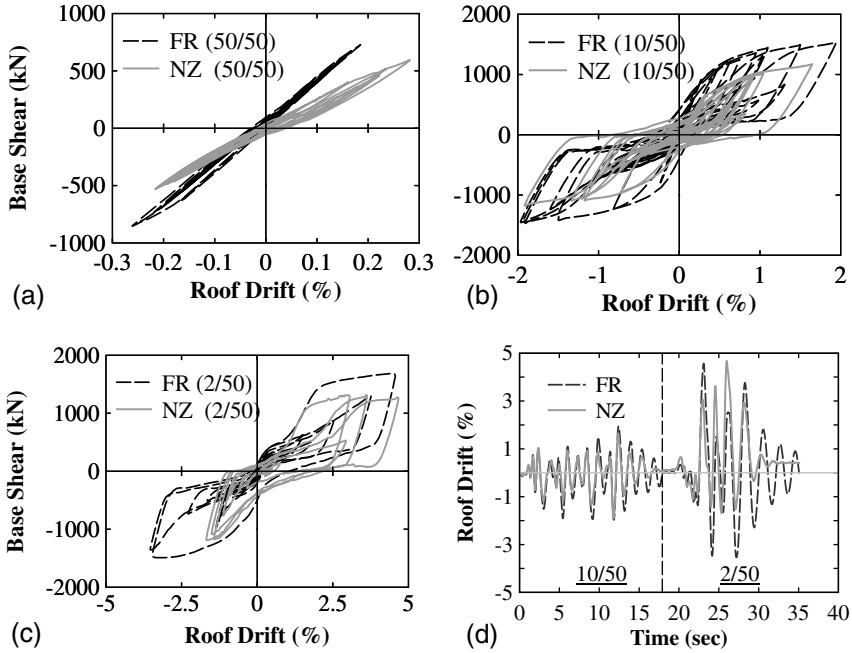

Fig. 6. Global system response: PSD

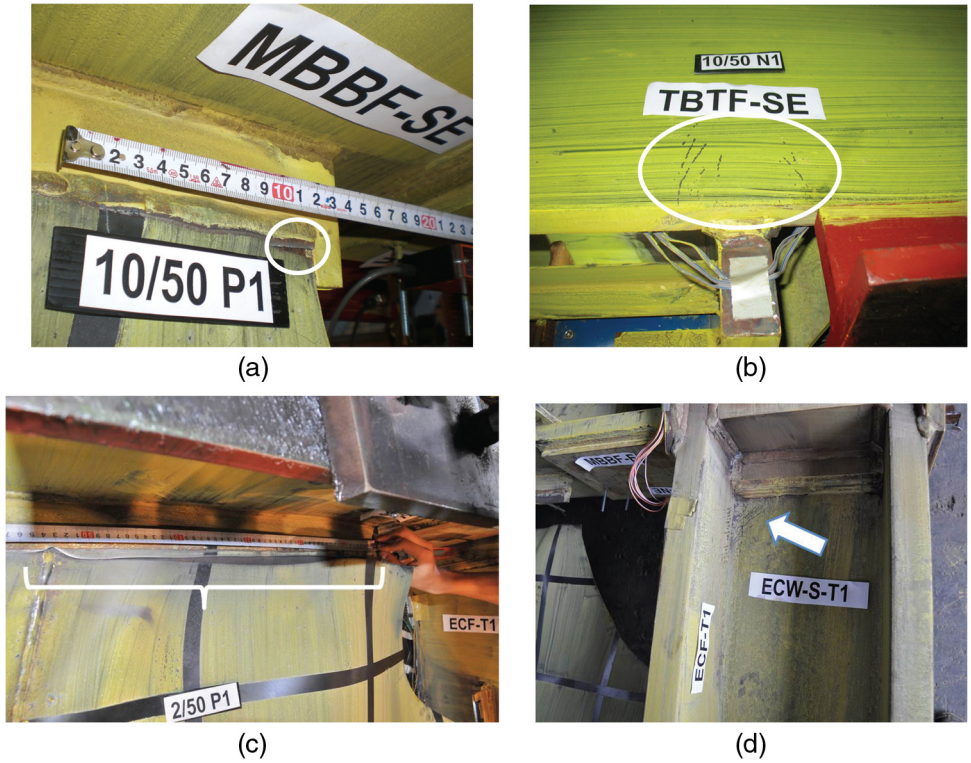

Fig. 7. Experimental observations: (a) small web plate tearing in specimen NZ during the 10/50 GM; (b) minor yielding the top beam of specimen NZ during the 2/50 GM; (c) approximately 40 cm web plate tearing in specimen FR during the 2/50 GM; (d) light yielding at the top of the first-story column of specimen FR during the 2/50 GM

indicate that both specimens had low residual drift, with Specimen FR achieving recentering (residual drift less than 0.2%). Note that recentering was not a performance objective for the 2/50 hazard level.

4. PSD test data show that both specimens achieved all performance objectives for all hazard levels.
5. For both specimens, the global response data for the 10/50 and 2/50 GMs indicate that the web plate has a nonnegligible residual strength when unloading from large drifts. This is shown by instances of nonzero base shear at zero drift and is consistent with observations made from subassemblage and scaled SC-SPSW tests described in Clayton (2013) and

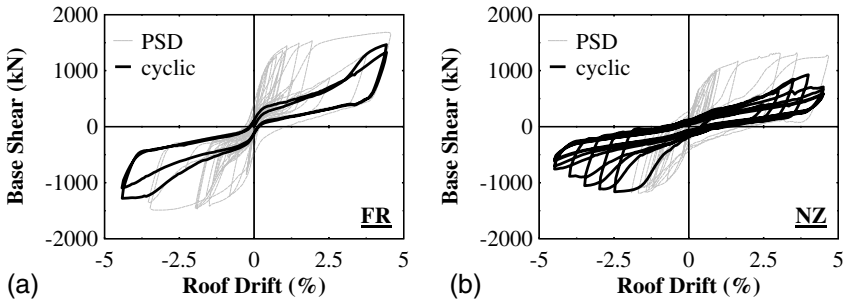

Fig. 8. Global system response: quasi-static

Dowden and Bruneau (2014), respectively. Webster (2013) investigated this web plate behavior and concluded it was due to the plastic contraction of the web plate in the direction perpendicular to the tension field direction. The experimental data presented here suggest that this residual web plate strength does not have a significant influence on frame recentering under earthquake excitations as it decays in magnitude as the amplitude of oscillation decays during free vibration. Similar results were observed in shake-table tests by Dowden and Bruneau (2014).

6. Note that in an actual building with SC-SPSWs, web plates would be essentially undamaged prior to a 2/50 earthquake; thus, the larger initial stiffness and energy dissipation provided by the undamaged web plate would reduce peak drifts from those observed in these laboratory tests. In other words, the 2/50 PSD test results are conservative, since should a 10/50 earthquake occur in practice, it is expected that the infill web plate would have been replaced prior to the occurrence of a subsequent 2/50 earthquake event.

Response of PT Elements

Figs. 9 and 10 show typical PT force versus roof drift histories for the test specimens. Fig. 9 shows the measured and predicted response based on analytical equations (Clayton 2013; Dowden and Bruneau 2014) for the PT strands at the top beam. Note that the predicted PT force response is based on the simplifying assumption that beam-to-column joint rotation is equal to roof drift ratio. Furthermore, for Specimen NZ, since the beam PT is anchored at points within the beam span, two beam PT response curves are shown. Fig. 10 shows the measured response for the column PT strands. The data in Figs. 9 and 10 support the following observations:

1. For Specimen FR, the beam PT force increases with increasing roof drift and is approximately symmetric in the positive and negative drift directions. This is typical for PT beam-to-column connections that rock about the top and bottom beam flanges.
2. For Specimen NZ, in the positive drift direction, the PT force at the closing joint (east end) reduces with increasing drift and eventually becomes fully relaxed due to the characteristics of the NewZ-BREAKSS connection. In the negative drift direction, the response of the PT at the closing joint (west end) does not mirror that response perfectly. This discrepancy is an artifact of the test setup. In the test setup, the actuators load the test specimen by pushing and pulling on the top of the west column (Fig. 1). Because the beam PT is anchored to the outside of the column, when the actuators pull on the west column to produce a negative roof drift, the actuators are also pulling on the west end beam PT. Thus, the west end beam PT is always in tension (which would not be otherwise).
3. The simplifying assumption used in the analytical predictions that the beam-to-column joint rotation is equal to roof drift ratio, provides a good but upper-bound estimate of PT load. Furthermore, the analytical equations are also conservative for the reason that PT force losses due to anchor wedge seating are not accounted for. Thus, these simplifying assumptions are appropriate for estimating PT demands for design.
4. The data in Fig. 10 show column PT force histories that are similar to the Specimen FR beam PT force histories shown in Fig. 9(a). This supports the previous assertion that that column base rocking connection [Fig. 4(c)] has kinematics similar to that of beam-to-column connections of Specimen FR.
5. For both the beam and column PT, the force versus drift histories are nonlinear even though the PT strands themselves remained elastic. This is due to the change in the axial force in the boundary frame members resulting from development and relaxation of web plate tension field action.
6. For Specimen FR, beam PT force is a minimum at zero drift; however, the column PT is not. This is due to the influence of the frame overturning moment on column axial forces

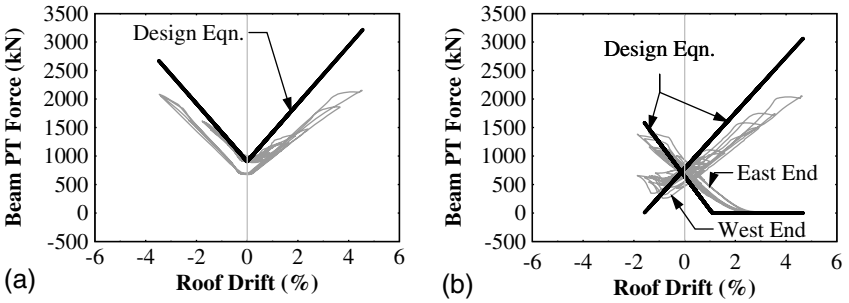

Fig. 9. Top beam PT force response for all PSD ground motions: (a) FR; (b) NZ

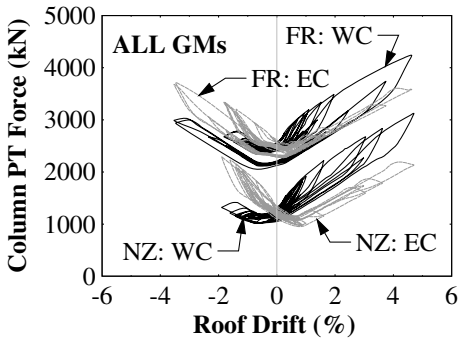

Fig. 10. Typical column PT force response for all PSD ground motions

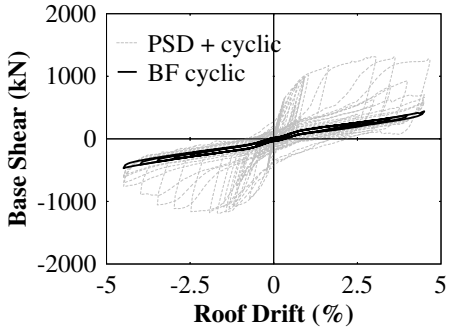

Fig. 11. Specimen NZ: PT boundary frame global system response

(which also has the same effect on Frame NZ columns). As the specimen is loaded, the compression and tension (or reduction in compression) developed in the columns due to the overturning moment cause the columns to shorten and elongate, respectively, resulting in a reduction of the PT force in the *compression* column and an increase in the PT force in the *tension* column.

PT Boundary Frame Response

For Specimen NZ, after the completion of the PSD and inelastic cyclic tests, the web plates were removed and additional cyclic tests were performed on the PT boundary frame. The global base shear versus roof drift and PT load versus roof drift are shown in Figs. 11 and 12, respectively. Results in Fig. 11 show that: (1) the energy dissipation provided by the boundary frame is insignificant; (2) the PT boundary frame provides approximately 30% of the total base shear strength of the SC-SPSW (analysis results are similar for the Specimen FR); and (3) the PT load versus roof drift response of the NZ boundary frame is essentially nonlinear elastic in the absence of the web plates. Furthermore, Fig. 12 more clearly shows the impact of the actuator pulling on the top beam PT in the negative drift direction (i.e., in the negative drift direction, the west end beam PT increases at approximately 1% drift) along with the overturning moment effects on the column PT response presented earlier.

For Specimen FR, the moment and axial force demands in the beams were calculated from strain gauges located along the length of the beam (Clayton 2013). Axial force (negative values indicating compression) and moment demands are shown for the middle beam in Table 3, where the moment is theoretically zero at the middle of the beam due to equal web plate strengths above and below the beam. The beam demands were measured at the middle of the beam [indicated as (M) in Table 3] and at locations 0.5 m (approximately 17% of the beam length) from the east and west ends of the beams [indicated as (E) and (W), respectively, in Table 3] such that they were sufficiently far from the connection region. The measured moment and axial demands at 2% roof drift presented in Table 3 are compared to those predicted from the design equations presented in Dowden et al. (2012). These equations are based on capacity design principles of yielding of the infill web plate only; the derived closed form equations that describe the moment, shear, and axial demand along the length of the beam of an SC-SPSW were obtained through first principles using detailed free body diagrams and validated with nonlinear cyclic pushover analysis of simple SC-SPSW frames. Due to space constraints, these equations are not repeated here. Additional discussion of the beam axial force

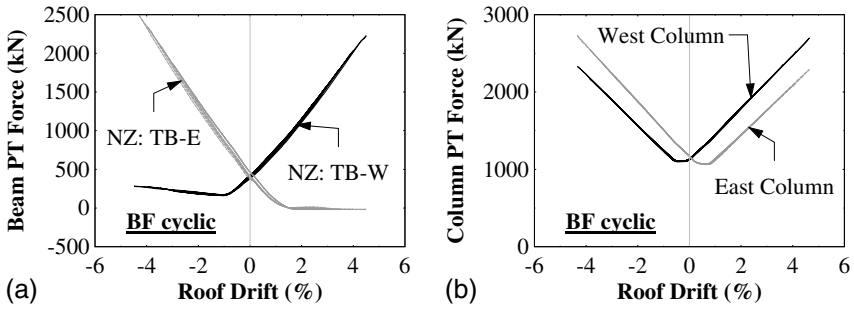

Fig. 12. Specimen NZ PT boundary frame response: (a) top beam PT; (b) column PT

Table 3. Beam Axial and Moment Demands for Specimen FR at 2% Drift

Beam	Demand (location)	Design equations	Experiment	Design equation/experimental
Top beam	Axial (M)	−2,760 kN	−2,170 kN	1.27
	Moment (M)	375 kN · m	302 kN · m	1.24
Middle beam	Axial (M)	−2,540 kN	−2,450 kN	1.04
	Moment (E)	−420 kN · m	−341 kN · m	1.23
	Moment (W)	420 kN · m	322 kN · m	1.30

and moment response can be found in Clayton et al. (2012b, 2013) and Dowden and Bruneau (2014). The axial and moment demands are not shown for Specimen NZ as these values were more difficult to derive from strain gauge data due to the close proximity of concentrated stresses due to the interior PT anchorage, and the difficulty in estimating initial PT force demands.

Note that the design axial load distribution presented in Dowden et al. (2012) was adjusted for the top beam to account for the applied story shear force acting only on one column (Moghimi and Driver 2014). Also, the beam demand equations in Dowden et al. (2012) are intended for design and therefore include conservative approximations, including the beam rocking depth being equal to the distance to the extreme fiber of the beam flange reinforcing plate and the gap opening being approximated as the story drift demand. Thus, the design equations represent a reasonable and conservative estimation of beam demands, overestimating measured demands by approximately 4–30% as indicated in Table 3.

Summary and Conclusions

Pseudodynamic tests were conducted on two full-scale two-story SC-SPSW specimens. The two specimens investigated different beam-to-column PT rocking connections: a flange-rocking (FR) connection and the NewZ-BREAKSS (NZ) connection (proposed to eliminate frame expansion and the need for the complex detailing to accommodate it in actual buildings). A comparison of the PT force and global lateral strength responses from both specimens demonstrated some of the differences in behavior of frames detailed with these connections. The specimens also both included PT column base details that provided additional recentering and allowed the columns to rotate without developing plastic hinges, as an alternative to using a clevis and pin connection.

The test program demonstrated that the SC-SPSW system is capable of meeting proposed performance objectives for buildings in areas of high seismicity. Both specimens had essentially elastic performance under excitation representing a 50/50 event, recentering, and yielding concentrated in the web plates following a 10/50 excitation, and minimal frame yielding and very small residual drifts following a 2/50 excitation. Experimental moment and axial force demands determined from strain gauges along the beams in Specimen FR demonstrated that the design equations presented in Dowden et al. (2012) provided reasonable and conservative estimations of flange-rocking beam demands at design-level drift ratios. These tests provide full-scale proof-of-concept that SC-SPSW systems can be a viable lateral-force-resisting system. The results also suggest that the boundary frame member sizes could be reduced while still maintaining desired levels of seismic performance; however, further research would be required to validate this.

Acknowledgments

Financial support for this study was provided by the National Science Foundation (NSF) as part of the George E. Brown Network for Earthquake Engineering Simulation under award number CMMI-0830294 and by the National Center for Research on Earthquake Engineering (NCREE) in Taiwan. P. Clayton was also supported by the NSF East Asia and Pacific Summer Institute program under award number OISE-1209569 and by the NSF Graduate Research Fellowship under award number DGE-0718124. Additional financial support for D. Dowden was provided by MCEER. The authors would also like to acknowledge material donations from the American Institute of Steel Construction and the hard work from NCREE staff and technicians for making these tests possible. Any opinions, findings, conclusions, and recommendations presented in this paper are those of the authors and do not necessarily reflect the views of the sponsors.

References

ASCE. (2010). "Minimum design loads for buildings and other structures." *ASCE/SEI 7–10*, Reston, VA.

Baldvins, N., Berman, J. W., Lowes, L. N., and Janes, T. (2012). "Development of damage prediction models for steel plate shear walls." *Earthquake Spectra*, 28(2), 405–426.

Chi, H., and Liu, J. (2012). "Seismic behavior of post-tensioned column base for steel self-centering moment-resisting frame." *J. Constr. Steel Res.*, 78, 117–130.

Chopra, A. K. (2007). *Earthquake dynamics of structures: Theory and applications to earthquake engineering*, 3rd Ed., Prentice Hall, Upper Saddle River, NJ.

Christopoulos, C., Filiatrault, A., Uang, C. M., and Folz, B. (2002). "Post-tensioned energy dissipating connections for moment-resisting steel frame." *J. Struct. Eng.*, 10.1061/(ASCE)0733-9445(2002)128:9(1111), 1111–1120.

Clayton, P. M. (2013). "Self-centering steel plate shear wall: Subassembly and full-scale testing." Ph.D. dissertation, Dept. of Civil and Environmental Engineering, Univ. of Washington, Seattle.

Clayton, P. M., Berman, J. W., and Lowes, L. N. (2012a). "Seismic design and performance of self-centering steel plate shear walls." *J. Struct. Eng.*, 10.1061/(ASCE)ST.1943-541X.0000421, 22–30.

Clayton, P. M., Berman, J. W., and Lowes, L. N. (2013). "Subassembly testing and modeling of self-centering steel plate shear walls." *Eng. Struct.*, 56, 1848–1857.

Clayton, P. M., Tsai, C.-Y., Berman, J. W., and Lowes, L. N. (2015). "Comparison of web plate numerical models for self-centering steel plate shear walls." *Earthquake Eng. Struct. Dyn.*, in press.

Clayton, P. M., Winkley, T. B., Berman, J. W., and Lowes, L. N. (2012b). "Experimental investigation of self-centering steel plate shear walls." *J. Struct. Eng.*, 10.1061/(ASCE)ST.1943-541X.0000531, 952–960.

Clifton, G. C., MacRae, G. A., Mackinven, H., Pampanin, S., and Butterworth, J. (2007). "Sliding hinge joints and subassemblies for steel moment frames." *Proc., New Zealand Society of Earthquake Engineering Annual Conf.*, Palmerston North, New Zealand.

Dowden, D. M., and Bruneau, M. (2011). "NewZ-BREAKSS: Post-tensioned rocking connection detail free of beam growth." *AISC Eng. J.*, 48(2), 153–158.

Dowden, D. M., and Bruneau, M. (2014). "Analytical and experimental investigation of self-centering steel plate shear walls." *Tech. Rep. MCEER-14-0010*, Multidisciplinary Center for Earthquake Engineering Research, State Univ. of New York Buffalo, Buffalo, NY.

Dowden, D. M., Purba, R., and Bruneau, M. (2012). "Behavior of self-centering steel plate shear walls and design considerations." *J. Struct. Eng.*, 10.1061/(ASCE)ST.1943-541X.0000424, 11–21.

FEMA (Federal Emergency Management Agency). (2000). "State of the art report on systems performance of steel moment frames subject to earthquake ground shaking." *Technical Rep. 355c*, SAC Joint Venture for Federal Emergency Management Agency, Washington, DC.

Garlock, M., Ricles, J., and Sause, R. (2005). "Experimental studies of full-scale posttensioned steel connections." *J. Struct. Eng.*, 10.1061/(ASCE)0733-9445(2005)131:3(438), 438–448.

Khoo, H. H., Clifton, G. C., Butterworth, J. W., and Mathieson, C. D. (2011). "Development of the self-centering sliding hinge joint." *Proc., Ninth Pacific Conf. on Earthquake Engineering Building an Earthquake-Resilient Society*, Auckland, New Zealand.

Li, C.-H., Tsai, K.-C., and Lee, H.-C. (2014). "Seismic design and testing of the bottom boundary vertical boundary elements in steel plate shear walls. Part 2: Experimental studies." *Earthquake Eng. Struct. Dyn.*, 43(14), 2155–2177.

MacRae, G. A., Clifton, G. C., and Butterworth, J. W. (2009). "Some recent New Zealand research on seismic steel structures." *STESSA09*, CRC Press, Philadelphia.

Mander, T. J., Rodgers, G. W., Chase, J. G., Mander, J. B., MacRae, G. A., and Dhakal, R. P. (2009). "Damage avoidance design steel beam-column moment connection using high-force-to-volume dissipators." *J. Struct. Eng.*, 10.1061/(ASCE)ST.1943-541X.0000065, 1390–1397.

Moghimi, H., and Driver, R. G. (2014). "Beam design force demands in steel plate shear walls with simple boundary frame connections." *J. Struct. Eng.*, 10.1061/(ASCE)ST.1943-541X.0000993, 04014046.

Newmark, N. M. (1959). "A method of computation for structural dynamics." *J. Eng. Mech.*, 85(3), 67–94.

Sommerville, P., Smith, N., Punyamurthula, S, and Sun, J. (1997). "Development of ground motion time histories for phase 2 of the FEMA/SAC steel project." *Technical Rep. SAC/BD-97/04*, SAC Joint Venture, Sacramento, CA.

Villaverde, R. (2009). *Fundamental concepts of earthquake engineering*, CRC Press, Boca Raton, FL.

Webster, D. J. (2013). "The behavior of un-stiffened steel plate shear wall web plates and their impact on the vertical boundary elements." Ph.D. dissertation, Dept. of Civil and Environmental Engineering, Univ. of Washington, Seattle.